

HD-R138 127

A COMPARISON OF SIGNAL-TO-NOISE RATIOS FOR  
NEAR-INFRARED DETECTORS(U) INDIANA UNIV AT BLOOMINGTON  
DEPT OF CHEMISTRY J E FREEMAN ET AL 30 JAN 84

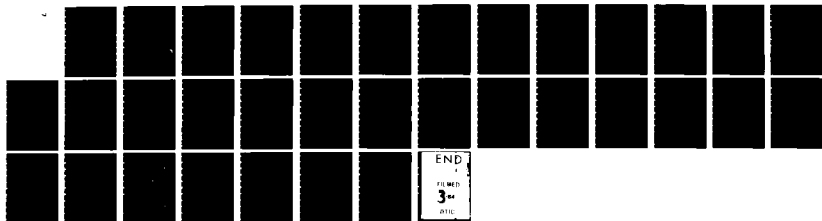
1/1

UNCLASSIFIED

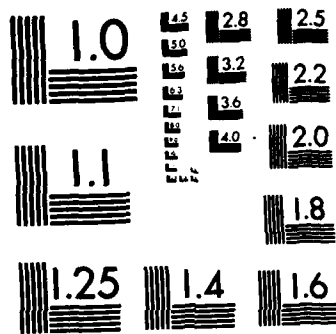
INDU/DC/GMH/TR-84-59 N00014-76-C-0838

F/G 17/5

NL



END  
FILMED  
3  
DTIC



MICROCOPY RESOLUTION TEST CHART  
NATIONAL BUREAU OF STANDARDS-1963-A

UNCLASSIFIED

12

SECURITY CLASSIFICATION OF THIS PAGE (When Data Entered)

REPORT DOCUMENTATION PAGE		READ INSTRUCTIONS BEFORE COMPLETING FORM
1. REPORT NUMBER INDU/DC/GMH/TR-84-59	2. GOVT ACCESSION NO.	3. RECIPIENT'S CATALOG NUMBER
TITLE (and Subtitle) A Comparison of Signal-to-Noise Ratios for Near-Infrared Detectors		5. TYPE OF REPORT & PERIOD COVERED Interim Technical Report
AUTHOR(s) J. E. Freeman and G. M. Hieftje		6. PERFORMING ORG. REPORT NUMBER 68
PERFORMING ORGANIZATION NAME AND ADDRESS Department of Chemistry Indiana University Bloomington, IN 47405		8. CONTRACT OR GRANT NUMBER(s) N14-76-C-0838
CONTROLLING OFFICE NAME AND ADDRESS Office of Naval Research Washington, D.C.		10. PROGRAM ELEMENT, PROJECT, TASK AREA & WORK UNIT NUMBERS NR 051-622
MONITORING AGENCY NAME & ADDRESS (if different from Controlling Office)		12. REPORT DATE 30 January 1984
		13. NUMBER OF PAGES 27
		15. SECURITY CLASS. (of this report) UNCLASSIFIED
		15a. DECLASSIFICATION/DOWNGRADING SCHEDULE

16. DISTRIBUTION STATEMENT (of this Report)  
This document has been approved for public release and sale; its distribution is unlimited.

17. DISTRIBUTION STATEMENT (of the abstract entered in Block 20, if different from Report)

18. SUPPLEMENTARY NOTES  
Prepared for publication in APPLIED SPECTROSCOPY

DTIC  
LECTE  
FEB 22 1984

19. KEY WORDS (Continue on reverse side if necessary and identify by block number)  
photodetectors  
near-infrared  
signal-to-noise ratio  
elemental analysis

20. ABSTRACT (Continue on reverse side if necessary and identify by block number)  
Five detectors sensitive in the near-infrared, including two photomultiplier tubes, a silicon photodiode, a silicon photodiode array, and a lead-sulfide photoconductor, are evaluated in terms of signal-to-noise ratios. Theoretical noise and signal calculations are compared to measured noise values and relative responses. The spectral response of the detectors between 700 and 1200 nm is also reported. The relative merits of a particular detector are a function of wavelength, photon flux and other criteria.

AD A138127

DTIC FILE COPY

OFFICE OF NAVAL RESEARCH

Contract N14-76-C-0838

Task No. NR 051-622

**A COMPARISON OF SIGNAL-TO-NOISE RATIOS FOR NEAR-INFRARED DETECTORS**

by

J. E. Freeman and G. M. Hieftje

**Prepared for Publication**

in

**APPLIED SPECTROSCOPY**

**Indiana University  
Department of Chemistry  
Bloomington, Indiana 47405**

30 January 1984

**Reproduction in whole or in part is permitted for  
any purpose of the United States Government**

**This document has been approved for public release  
and sale; its distribution is unlimited**

## INTRODUCTION

Recent research with analytically useful noble-gas plasmas has included an examination of the near-infrared spectral region (700-2000 nm) for the detection of atomic emission (1-4). Such plasmas possess sufficient energy to electronically excite and/or ionize even nonmetals, which have large excitation and ionization potentials compared to those of metal atoms. Nonmetals are of particular interest, since many do not possess intense atomic emission lines in the ultraviolet-visible spectral region above 200 nm. There are many potentially useful atomic lines in the near-infrared for elements such as carbon, nitrogen, oxygen, sulfur, chlorine, and bromine. The existence of these lines and the relative absence of band spectra and background emission suggest the possibility of exploiting near-infrared atomic emission for analytical purposes.

The principal problem with near-infrared emission spectroscopy is the lack of high-responsivity, low-noise detectors. Few, if any, near-infrared detectors approach the performance of photomultipliers used in the ultraviolet-visible spectral region. The Ag-O-Cs photocathode, which enables near-infrared response for some photomultipliers, possesses a lower quantum efficiency (by a factor  $> 10$ ) and a larger dark current (by a factor  $> 100$ ) than more conventional photocathodes. Semiconductor detectors sensitive in the near-infrared lack the internal gain of photomultipliers and thus require high gain, low noise amplifiers. Many such detectors will themselves, exhibit high noise levels.

In order to properly evaluate any near-infrared emission technique the correct detector must be chosen. This paper discusses theoretical signal and noise expressions and presents experimental signal and noise measure-



Avail and/or Special
Y Codes

ments for five detectors sensitive in the near-infrared: two photomultiplier tubes (PMTs), a silicon photodiode (PD), a PbS photoconductive detector (PCD), and a linear silicon photodiode array (PDA). In addition, spectral response curves for these detectors between 700 and 1200 nm are presented. The detector of choice for a particular application is found to depend on a number of measurement parameters including the spectral region of interest and the photon flux to be detected.

## THEORY

Definitions for symbols used in this discussion are given in Table I.

The five detectors to be considered are all photon detectors; that is, incident photons act in a discrete manner to produce free charge carriers. Photoemission from the photocathode of the PMTs produces electrons, which are accelerated and multiplied in the dynode chain. The photovoltaic effect, which describes the operation of the PD and PDA, involves the separation of photon-produced charge carriers on either side of a semiconductor junction. The photoconductive effect involves a change in semiconductor conductivity produced when incident photons create free charge carriers. There is no p-n junction in a photoconductive semiconductor.

Expressions for the signal voltage from the PMTs, PD, and PCD are given by Equations 1, 2, and 3, respectively (5-7). The signal

$$S_{\text{PMT}} = R_1 \phi A \eta_k(\lambda) \eta_d e G \quad (1)$$

$$S_{\text{PD}} = R_1 \phi A \eta e \quad (2)$$

$$S_{\text{PCD}} = \frac{V_b R_1 (\Delta R_d)}{(R_1 + R_d)^2} \quad (3)$$

expressions for the PMTs and PD are functions of quantities which are either known or easily estimated. The PCD signal expression is a function of  $\Delta R_d$ , the change in resistance of the PCD produced by incident photons. This resistance change is, in turn, a function of various parameters including the free charge carrier concentration and lifetime (6). The PDA is an integrated circuit configured such that detector current does not flow through a load resistor, but instead charges a capacitor: the PDA is an integrating detector.

A number of potentially significant noise sources must be considered; their relative importance depends on the detector type and modulation frequency. In general, one noise source will predominate, although the predominant source may change with frequency and incident photon flux. Johnson noise in a load resistor or amplifier feedback resistor can be calculated from the Nyquist formula (5-7),

$$\sigma_{J, \text{PMT/PD}} = [4kTR_1 \Delta f]^{1/2} . \quad (4)$$

Equation 4 yields valid noise calculations for the PMTs and PD, which have internal resistances much greater than  $R_1$ . For the PCD the parallel resistance of the detector and load resistor must be used, since  $R_1$  and  $R_d$  are usually comparable. Equation 5 allows the calculation of Johnson noise in this case and includes a correction for the temperature of the (normally cooled) PCD (5).

$$\sigma_{J, \text{PCD}} = \left[ 4k \frac{R_d R_1}{(R_d + R_1)^2} (R_d T_d + R_1 T_r) \Delta f \right]^{1/2} \quad (5)$$

Shot noise arises from the random character of discrete events, such as the arrival of photons at a detector, the emission of photoelectrons from a photocathode, or the passage of charge carriers across a p-n junction. Shot noise calculations usually distinguish between photon and dark (thermionic emission, thermal generation of charge carriers) noise sources. Equations 6 and 7 are shot noise expressions for the PMTs and PD, respectively (7,8).

$$\sigma_{S,PMT} = R_1 [2eBG^2\eta_d(i_p + i_d) \Delta f]^{1/2} \quad (6)$$

$$\sigma_{S,PD} = R_1 [2e(i_p + i_d) \Delta f]^{1/2} \quad (7)$$

For the PMTs it is assumed that only thermionic emission from the photocathode is a significant dark noise source; thus  $i_p$  and  $i_d$  are both photocathode currents. Shot noise in the PCD is usually termed "generation-recombination" noise, which refers to the random generation and recombination of charge carriers in the semiconductor. A detailed description of generation-recombination noise requires knowledge of charge carrier lifetimes and mobilities (5). Photon-induced shot noise in the PCD can be calculated using equation 7. The factor B in equation 6 accounts for additional noise caused by the statistical nature of electron emission from the PMT photocathodes. B can be calculated from equation 8,

$$B = \sum_{j=0}^m g^{-j} \quad (8)$$

where  $g$  is the average gain per dynode stage ( $g = G^{1/m}$ ) and  $m$  is the number of stages (8). Ordinarily, an additional correction for thermionic emission from dynodes is necessary; however, low-work-function photocathodes are the dominant source of thermionic emission in near-infrared-sensitive PMTs.

Flicker noise, which is inversely dependent on modulation frequency, is poorly understood. It can arise from a variety of sources including the

bias voltage supply, dynode resistors, detector resistance, and semiconductor detectors themselves. Although flicker noise is frequently significant, an exact and general expression for its calculation is not available.

The preamplifier used with each detector will also contribute noise to all measurements. Amplifier noise can be calculated using equation 9

$$\sigma_A = [(R_1^2 i_a^2 + V_a^2) \Delta f]^{1/2} \quad (9)$$

and equivalent input noise current and voltage specifications (9). Amplifier noise usually contains a flicker-noise component which is reflected in the equivalent input noise specifications at low frequencies.

Noise sources other than those mentioned above, such as ionizing radiation and readout noise, are assumed to be negligible for the PMTs PD, and PCD.

The integrating nature of the PDA necessitates the use of different signal and noise expressions. These expressions are customarily given in terms of the number of electrons or charge placed on the integrating capacitor at a single pixel. The signal expression for a PDA is given by equation 10, which is merely equation 2 recast in terms of the number of electrons.

$$n_{PDA} = \phi A n t \quad (10)$$

The dominant noise source in the silicon PDA is fixed-pattern noise resulting from clock-pulse coupling onto the video lines. At constant temperature and integration time this noise can be subtracted, and will no longer be a limiting noise source. Simpson (10) has presented equations for the significant noise sources in the PDA, expressed in terms of number of elec-

trons; equations 11 and 12 give the expressions for dark current shot noise and amplifier noise.

$$n_{S,PDA} = \left[ \frac{(i_p + i_d)t}{e} \right]^{1/2} \quad (11)$$

$$n_{A,PDA} = \left( \frac{1}{e} \right) [(i_a t_p)^2 + (v_a C)^2]^{1/2} \quad (12)$$

(The total capacitance, C, is the sum of video line, amplifier, and stray capacitance.) Readout noise, which is related to the process of switching pixels onto and off from the video line, is described by equation 13.

$$n_{R,PDA} = \left( \frac{1}{e} \right) [kT_d(2C_p + 2C_{vc})]^{1/2} \quad (13)$$

The PDA signal-processing circuit includes an external scaling preamplifier, a sample-and-hold unit, and an analog-to-digital converter (ADC). Scaling preamplifier noise can be calculated using equation 9. The rms quantization noise contributed by the ADC will be  $1/\sqrt{12}$  times the magnitude of the quantization level (11).

#### EXPERIMENTAL

Signal and noise measurements were made for each of four detectors (PMTs, PD, and PCD) using the apparatus depicted in Figure 1. Radiation from a tungsten-strip lamp (Model 18A/T10/2P, General Electric Co., Cleveland, OH) was focused with a 10-cm focal length quartz lens onto the entrance slit of a 0.35-m Czerny-Turner monochromator (Model EU-700, GCA

McPherson, Acton, MA). The monochromator was equipped with a 600 groove/mm grating blazed at 1000 nm and had entrance and exit slits fixed at 0.1 mm. The lamp was operated at a temperature of approximately 1400°K, determined by calibration against an NBS standard lamp (No. 431-P-717). The radiation was modulated at 153.4 Hz, a frequency remote from interference noise, by a mechanical chopper (Model 7505, Rofin, Marlboro, MA) placed between the lens and monochromator.

The PCD was a 2-mm x 2-mm square lead-sulfide detector equipped with a two-stage thermoelectric cooler and a calibrated thermistor for measuring the detector temperature (Model 2757 TCD, Infrared Industries, Waltham, MA). The PD was a 1-mm-diameter silicon p-i-n photodiode (Model 5082-4207, Hewlett Packard, Palo Alto, CA). Both the PCD and PD were mounted on brass housings which could accept a laboratory-constructed preamplifier assembly. The first photomultiplier (Model 7102, Hamamatsu, Middlesex, NJ), a ten-stage, end-on tube with a Ag-O-Cs photocathode and a gain of  $2.0 \times 10^5$ , was mounted in a thermoelectrically-cooled housing (Models 7102/117 and TE104RF-002, Products for Research, Danvers, MA) using tap water as a heat-exchange medium. The second photomultiplier (Model R636, Hamamatsu, Middlesex, NJ), a nine-stage, side-on tube with a GaAs(Cs) photocathode and a gain of  $1.6 \times 10^5$ , was mounted in a room-temperature housing (Model 3150, Pacific Precision Instruments, Concord, CA). During signal measurements with each PMT, a 1-mm-diameter aperture was placed at the exit slit to restrict the slit height to the size of the PD.

Each detector was connected, in turn, to the same preamplifier, which consisted of an ac-coupled operational amplifier (Model LF356, National Semiconductor, Santa Clara, CA) configured as a voltage follower with an effective load resistance of  $6.7 \times 10^6$  (Figure 2). The preamplifier and a reference signal output from the chopper were connected to a lock-in ampli-

fier (Model 5101, Princeton Applied Research, Princeton, NJ). Both filter stages on the lock-in amplifier were set for a time constant of 1s, giving an equivalent noise bandwidth of 0.125 Hz. Equivalent noise bandwidth is defined as the bandwidth of a boxcar function with height equal to the maximum response of the measurement system and area equal to that of the total noise power spectrum. Measurements were traced on a strip-chart recorder (Model SR-204, Heath, Benton Harbor, MI). Detector bias voltages of -50 V, -10 V, and -1250 V for the PCD, PD, and PMTs respectively, were supplied by a high-voltage power supply (Model 415B, Fluke, Seattle, WA). DC measurements for the PMTs were made using a picoammeter (Model 414S, Keithley, Cleveland, OH), a 1-s time-constant low-pass filter, and the strip-chart recorder.

Signal measurements were made with the lamp on and the monochromator set at 900 nm. Noise measurements for the detectors were made with the lamp off and the entrance slit blocked. Additional noise measurements were made for various components by removing the detectors, load resistors, etc. The rms noise voltages were taken to be one-fifth of the peak-to-peak noise amplitude measured for a duration of at least one-hundred time constants.

The PDA (Model 1024S, EG&G Reticon, Sunnyvale, CA) was an integrated circuit consisting of a linear array of 1024 pixels, each of which had a height of 2.5 mm and an effective width of 25  $\mu\text{m}$ . To facilitate alignment in the monochromator focal plane, the PDA was connected to its preamplifier circuit via a 40-cm length of ribbon cable. The preamplifier described above was not used with this detector; instead, the video signal from the PDA was processed by an evaluation circuit provided by the manufacturer (Model RC 1024S, EG&G Reticon, Sunnyvale, CA). The signal was further processed by a scaling preamplifier (Model AM 102B, Datel Intersil,

Mansfield, MA), a sample and hold unit (Model SHM-2, Datel Intersil, Mansfield, MA), and a twelve-bit ADC (Model ADC-EH12B1, Datel Intersil, Mansfield, MA). The digital output was stored by a MINC 11/23 computer (Digital Equipment Corporation, Maynard, MA). The scaling preamplifier was adjusted so that the PDA and the ADC were saturated at the same signal level.

The PDA was cooled to a temperature of approximately  $-17^{\circ}\text{C}$  by a two-stage thermoelectric cooler (Models SE 1012, ST 1021, and 1056, Marlow Industries, Garland, TX). Unmodulated radiation from the lamp was integrated on the detector for a period of 4s, giving an equivalent noise bandwidth of 0.125 Hz. A 1-mm aperture restricted the entrance slit height to that used with the PD and PMTs. Dark noise measurements were made by recording the fluctuations of a single pixel in the PDA. All PDA measurements were made after subtraction of a dark scan.

Spectral response curves for the PMTs, PD, and PCD were obtained by operating the tungsten lamp at a temperature of  $2200^{\circ}\text{K}$  and scanning the monochromator between 700 and 1200 nm. Scanning and data acquisition were controlled by a computer (Model PDP 11/34A, Digital Equipment Corp., Maynard, MA). The data were normalized using the Planck radiation law for a  $2200^{\circ}\text{K}$  blackbody source, and scaled according to the S/N values measured at 900 nm.

## **RESULTS AND DISCUSSION**

The results of noise calculations, based on equations discussed above, for each single-channel detector are presented in Table II. It should be emphasized that these calculations are for dark noise. Any real spectrophotometric measurement would include noise contributed by the photon

source. Calculations for the 7102 PMT and PCD under both room-temperature and cooled conditions are included. The operating temperatures chosen for all detectors are typical and are not necessarily optimal. The preamplifier and lock-in amplifier calculations are, naturally, the same in each case. These results indicate that the PMTs should be shot-noise limited under both room-temperature and cooled conditions, whereas the PD should be limited by Johnson noise in the load resistor. The necessary omission of flicker noise calculations is crucial, since the PCD is certainly dominated by noise of that type. For this reason no meaningful signal-to-noise calculations can be made for that detector. Importantly, the magnitude of flicker noise is a strong function of the detector area (5). A PCD should have as small an area as is practical for a given application. Because dark current is a function of detector area, shot-noise values for all detectors are dependent on detector area as well.

Noise calculations for the PDA, expressed both as a number of electrons and as a fraction of saturation charge, are presented in Table III. (The saturation charge is specified to be 14 pcoul, which is equivalent to  $8.8 \times 10^7$  electrons. The preamplifier and ADC outputs at saturation are 3 V and 4095 quantization units, respectively.) The fraction-of-saturation figures allow a convenient comparison with measured values and indicate the available dynamic range for signal integration. A minimally detectable signal value can be taken as the quadratic sum of the calculated noise values, which equals  $7.5 \times 10^{-5}$  times the saturation charge. The reciprocal of this number gives an approximate dynamic range of  $1.3 \times 10^4$ . The pixel readout and preamplifier noise calculations are probably too low: they require values for video-line and other capacitances which, because the array chip is separated from the evaluation circuit board by ribbon cable, are certainly much larger than specified. (The total capacitance, C, used in the calculation of preamplifier noise includes a rough estimate of the stray ribbon-cable capacitance.) Careful circuit design to minimize video-line capacitance and crosstalk is essential when the PDA must be separated from the

evaluation circuit. This separation is usually necessary in order to cool the PDA and mount it in a monochromator.

Table IV summarizes signal and total noise measurements for each detection system. These measurements do not include signal-induced noise and, hence, represent the limiting noise in a low-signal situation. The lamp temperature used to make signal measurements was chosen to be low enough to avoid saturation of the PDA. This requirement resulted in a signal which was well below the minimally detectable signal for the room-temperature PCD; thus, no signal measurements are included for that detector at room temperature.

The calculations of Table II predict a shot-noise limit for the PMTs; the measured noise voltages are within a factor of 2-3 of those calculated. A cursory examination of the frequency spectrum of 7102 PMT noise indicates some  $1/f$ -type behavior. Nevertheless, the signal-to-noise behavior of the 7102 PMT follows the square root relationship expected for shot noise: the S/N for DC measurements is just twice that for the 50-percent duty-cycle modulated measurements (again, signal-induced noise is not included), and a plot of  $S_{\text{PMT}}^{1/2}$  vs.  $\phi_{\text{PMT}}$  at various values of  $i_d$  gives a straight line.

The PD was predicted to be limited by Johnson noise in the preamplifier load resistance. The measured noise amplitude corresponds closely to the calculated value from Table II. In fact, independent measurements of noise in the preamplifier with and without the load resistance and in the lock-in amplifier pinpoint the load resistance as the limiting noise source. Without a detector the amplifier system noise is  $1.2 \times 10^{-7}$  V rms. Replacement of the load resistance with a  $100 \Omega$  input resistor reduces the noise to  $1.8 \times 10^{-8}$  V rms. The lock-in amplifier alone exhibits a noise amplitude of  $1.0 \times 10^{-8}$  V rms. (These last two values differ from calculated values by factors of 1.3 and 2.9.)

The measured noise amplitude for the PCD is, as expected, greater than any of the calculated values of Table II. The PCD is limited by flicker noise, and its noise power spectrum shows a strong  $1/f$  dependence at low frequencies.

The quadratic sum of the noise values calculated for the PDA (Table III) yields a value  $1.1 \times 10^{-4}$  times saturation charge for a background-subtracted signal whereas the measured quantity of  $9.3 \times 10^{-4}$  (Table IV) is a factor of 9 larger. This discrepancy might be due to the capacitance increase caused by separating the array chip from the evaluation circuit board. Another significant noise source could be the external preamplifier/sample-and-hold/ADC circuit, which alone exhibits a noise value, of  $3.9 \times 10^{-4}$  times saturation charge. This contribution is 4 times the calculated sum of scaling preamplifier and quantization noise. Obviously, improvements in the signal-recovery circuits for the PDA could significantly improve its noise characteristics.

A more important criterion than the absolute noise level is the signal-to-dark-noise ratio. Comparisons independent of photon flux can be made by calculating the ratio of two individual signal-to-dark-noise ratios using the signal expressions (equations 1, 2, and 10) and calculated noise values from Tables II and III. Such comparisons assume a low flux situation where photon-induced shot noise is not the dominant noise source. With  $\eta_k$  (900 nm) =  $2.4 \times 10^{-3}$  (19),  $\eta_d \approx 0.9$  (12), and  $\eta = 0.69$  (13), the S/N for the 7102 PMT should be 7.5 times the S/N for the PD. The quadratic sum of the calculated noise values for the PDA must include a factor of two, since PDA data are background-subtracted. When corrections are made for detector areas, the computed S/N for the PDA is 12 times that for the PD. Measured values for signal-to-dark-noise ratios at 900 nm are given in Table IV. The

ratio of these values for the PMT and PD are  $(8.2 \times 10^2)/(5.6 \times 10^2) = 1.5$ ; for the PDA and PD the ratio is  $(2.5 \times 10^2)/(5.6 \times 10^2) = 0.45$ . The PMT/PD values correspond within a factor of five to calculations, whereas the PDA/PD ratio is a factor of 27 smaller than predicted. If the calculated noise value for the PDA is replaced by the measured value, the calculated PDA/PD ratio, 1.4, is much closer to the measured result. The discrepancy is, as explained above, between the calculated and measured PDA noise values.

In practice, for extended sources, the much larger photosensitive area of the PMTs could be exploited to yield a significant increase in S/N. The PDA also has a larger available aperture ( $\times 2.5$ ) than that used for the present measurements. With careful circuit design the readout and amplifier noise values for the PDA should approach calculated values. Furthermore, the multichannel format of the PDA can increase its effective S/N in many measurement situations (20).

Ingle and Crouch have pointed out that a S/N comparison of a PMT and a PD depends on the incident photon flux (7,21), and that there is a crossover point below which the PMT exhibits a better S/N and above which the PD is better. Because silicon PDs have a large quantum-efficiency advantage over the Ag-O-Cs (7102 PMT) photocathode (0.69 vs. 0.0024 at 900 nm), this crossover should be shifted to lower light levels here than in the ultraviolet-visible region. The crossover point can be determined by plotting signal-to-noise ratios (equations 14 and 15) calculated using equations 1, 2, 4, 6, and 7.

$$S/N_{PMT} = \frac{S_{PMT}}{[\sigma_{J,PMT}^2 + \sigma_{S,PMT}^2 + \sigma_{A,PMT}^2]^{1/2}} \quad (14)$$

$$S/N_{PD} = \frac{S_{PD}}{[\sigma_{J,PD}^2 + \sigma_{S,PD}^2 + \sigma_{A,PD}^2]^{1/2}} \quad (15)$$

A similar calculation (equation 16) can be made for the PDA using equations

$$S/N_{PDA} = \frac{n_{PDA}}{[n_{S,PDA}^2 + n_{A,PDA}^2 + n_{R,PDA}^2]^{1/2}} \quad (16)$$

10-13. (Scaling preamplifier and quantization noise calculations have been omitted, in deriving equation 16, because they could be minimized in a well-designed readout system.) Equations 14, 15, and 16 are plotted in Figure 3 as a function of incident photon flux. (The calculations were made for a 900 nm light source image of 1-mm diameter focused onto a single detector element and for an equivalent noise bandwidth of 0.125 Hz.) The bend in the PD curve corresponds to the region where Johnson and shot noise contributions are comparable. The bend in the 7102 PMT curve corresponds to the region where shot noise caused by thermionic emission becomes significant. The crossover point occurs at a flux of  $2.0 \times 10^{10}$  photons  $s^{-1} cm^{-2}$ , which corresponds to a PMT anode current of  $1.3 \times 10^{-8}$  A. (This current is four orders of magnitude greater than the rms dark noise, which was measured to be  $1.0 \times 10^{-12}$  A for the cooled PMT.) The PDA should exhibit comparable or better S/N performance than either the 7102 PMT or the PD if the capacitance and signal recovery problems can be eliminated. The PDA does suffer from a more limited dynamic range: the upper limit in photon flux is determined by the pixel saturation charge. The upper limits for the 7102 PMT and PD are determined, respectively, by the maximum average anode current rating and a practical amplifier output voltage ( $\sim 10$  V). The corresponding S/N vs.  $\phi$  curve for the R636 PMT would almost exactly overlap that for the 7102 PMT,

the major difference being the much lower maximum average anode current of the R636 PMT, which would limit it to a maximum  $\log \phi$  of 11.6.

The signal-to-(detector) noise ratio is certainly not the only criterion to be considered in choosing the best near-infrared detector for a particular application. Spectral response is also an important consideration. Figure 4 is a plot of the spectral response for the two PMTs, the PD, and the PCD between 700 and 1200 nm. The curves have been scaled to reflect the S/N values measured at 900 nm. At any particular wavelength the ordinate value for the curves corresponds to the response at that wavelength divided by the detector (dark) noise. Clearly, the R636 PMT has a significant advantage below approximately 890 nm; however, the 7102 PMT or the silicon detectors would probably offer superior performance between 900 and 1100 nm. The PCD is probably the most useful detector beyond 1100 nm. (The PDA curve was eliminated for clarity: its response would mimic that of the silicon PD with an appropriate S/N offset.)

Other important criteria in choosing a near-infrared detector include dynamic range, the range of photon flux to be measured, readout complexity, the need for multichannel measurements, and cost. The cooled PDA, the cooled 7102 PMT and the R636 PMT all exhibit a S/N advantage over the PD at low light levels. This advantage would increase if the larger formats of these detectors were utilized. The limited spectral response of the R636 PMT precludes its use for some applications, such as the detection of sulfur emission above 900 nm (4). The PDA and PMTs are, however, considerably more expensive than the PD. Improvements in the PDA readout system would likely yield better S/N characteristics for that detector, although the dynamic range limitation caused by saturation remains a significant problem. The PD, on the other hand, exhibits a S/N advantage at high light fluxes. The

PCD would be the detector of choice only for measurements beyond approximately 1100 nm. The above discussion should indicate both the importance of S/N comparisons and the relative accuracy with which the necessary calculations can be made.

#### **ACKNOWLEDGEMENTS**

The authors are grateful for technical assistance from and helpful discussions about S/N with R. Withnell and R. E. Ensmann. One of the authors (J.E.F.) wishes to thank the Perkin-Elmer Corporation, the Analytical Division of the American Chemical Society, and Procter and Gamble for fellowship support during this investigation. This research was supported in part by the National Science Foundation and by the Office of Naval Research.

## REFERENCES

1. S. K. Hughes and R. C. Fry, *Anal. Chem.*, 53, 1111 (1981).
2. S. K. Hughes and R. C. Fry, *Appl. Spectrosc.*, 35, 493 (1981).
3. S. K. Hughes, R. M. Brown, Jr., and R. C. Fry, *Appl. Spectrosc.*, 35, 396 (1981).
4. J. E. Freeman and G. M. Hieftje, presented at FACSS, 1982.
5. P. W. Kruse, L. D. McGlauchlin, and R. B. McQuistan, Elements of Infrared Technology, John Wiley and Sons, New York, NY, 1962.
6. The Infrared Handbook, W. L. Wolfe and G. J. Zissis, eds., Office of Naval Research, Washington, D.C. (1978).
7. J. D. Ingle, Jr. and S. R. Crouch, *Anal. Chem.*, 43, 1331 (1971).
8. T. C. O'Haver and J. D. Winefordner, *Appl. Opt.*, 7, 1647 (1968).
9. J. D. Ingle, Jr. and S. R. Crouch, *Anal. Chem.*, 44, 785 (1972).
10. R. W. Simpson, *Rev. Sci. Instrum.*, 50, 730 (1979).
11. P. C. Kelly and Gary Horlick, *Anal. Chem.*, 45, 518 (1973).
12. A. T. Houngh and R. E. Schild, *Appl. Opt.*, 10, 1668 (1971).
13. PIN Photodiodes, 5082-4200 Series, Hewlett Packard, Palo Alto, CA (1980).
14. Linear Databook, National Semiconductor, Santa Clara, CA (1982).
15. Model 5101 Lock-in Amplifier Operating Source Manual, EG&G Princeton Applied Research, Princeton, NJ (1981).
16. S-Series Solid State Line Scanners, EG&G Reticon, Sunnyvale, CA (1978).
17. Transistor Databook, National Semiconductor, Santa Clara, CA (1982).
18. AM103B Data Sheet, Datel Intersil, Mansfield, MA (19 ).
19. Photomultiplier Tubes, Hamamatsu, Middlesex, NJ.

20. J. D. Winefordner, R. Auni, T. L. Chester, J. J. Fitzgerald, L. P. Hart, D. J. Johnson, and F. W. Plankey, *Spectrochim. Acta*, 31B, 1 (1976).
21. J. D. Ingle, Jr. and S. R. Crouch, *Anal. Chem.*, 44, 1709 (1972).

## FIGURE CAPTIONS

- Figure 1. Apparatus used to make signal measurements for the PMTs, PD and PCD.
- Figure 2. Preamplifier circuit used with the PMTs, PD, and PCD.
- Figure 3. S/N as a function of incident photon flux for the 7102 PMT ( $\bullet$ ), PD (+), and PDA ( $\star$ ). Calculated for a 900 nm light source image of 1-mm diameter focused onto a single detector element and for an equivalent noise bandwidth of 0.125 Hz.
- Figure 4. Relative spectral response divided by detector noise for the R636 PMT (a), 7102 PMT (b), PD (c), and PCD (d). Curve d is multiplied by 10. All curves are multiplied by 10 between 950 and 1200 nm.

Table I. Symbol Definitions

A	detector area
B	secondary emission statistical factor
C	total input capacitance of PDA video amplifier
$C_p$	PDA pixel capacitance
$C_{vc}$	PDA video-line-to-clock-line capacitance
e	electron charge
g	average PMT dynode gain
G	PMT current gain
$i_a$	amplifier equivalent input noise current
$i_d$	dark current
$i_p$	photon-induced current
k	Boltzmann's constant
m	number of PMT dynode stages
n	number of electrons for the PDA subscripts: PDA - signal; S,PDA - shot noise; A,PDA - amplifier noise; R,PDA - pixel-reset noise
$R_l$	load or feedback resistance in amplifier circuit
$R_d$	detector resistance
S	signal voltage subscripts: PMT - photomultiplier; PD - photodiode; PCD - photoconductive detector
t	PDA integration period
$t_p$	PDA readout time for one pixel
$T_d$	detector temperature
$T_r$	resistor temperature
$v_a$	amplifier equivalent input noise voltage
$V_b$	detector bias voltage
$\Delta f$	measurement system bandwidth
$\eta$	PD quantum efficiency
$\eta_d$	first dynode collection efficiency
$\eta_k(\lambda)$	photocathode quantum efficiency at wavelength $\lambda$
$\sigma$	rms noise voltage subscripts: J - Johnson noise; S - shot noise; A - amplifier noise; PMT, PD, PCD as under S
$\phi$	photon flux

Table II. Calculated Contributions to White Noise Output: Single Channel Detectors

Noise Source	Calculated Noise Values (V rms)					
	R636 PMT (23°C) <sup>1</sup>	7102 PMT (23°C) <sup>2</sup>	7102 PMT (cooled) <sup>3</sup>	PD (23°C) <sup>4</sup>	PCD (23°C) <sup>5</sup>	PCD (-30°C) <sup>6</sup>
Johnson	1.2 x 10 <sup>-7</sup>	1.2 x 10 <sup>-7</sup>	1.2 x 10 <sup>-7</sup>	1.2 x 10 <sup>-7</sup>	3.6 x 10 <sup>-8</sup>	6.4 x 10 <sup>-8</sup>
Shot (dark)	6.0 x 10 <sup>-6</sup>	3.4 x 10 <sup>-4</sup>	1.0 x 10 <sup>-5</sup>	6.7 x 10 <sup>-8</sup>	—	—
Preamplifier <sup>7</sup>	2.4 x 10 <sup>-8</sup>	2.4 x 10 <sup>-8</sup>	2.4 x 10 <sup>-8</sup>	2.4 x 10 <sup>-8</sup>	2.4 x 10 <sup>-8</sup>	2.4 x 10 <sup>-8</sup>
Lock-in Amplifier <sup>8</sup>	3.5 x 10 <sup>-9</sup>	3.5 x 10 <sup>-9</sup>	3.5 x 10 <sup>-9</sup>	3.5 x 10 <sup>-9</sup>	3.5 x 10 <sup>-9</sup>	3.5 x 10 <sup>-9</sup>

<sup>1</sup> $i_d = 5.9 \times 10^{-16} \text{A}$ ,  $B = 1.36$ ,  $G = 1.6 \times 10^5$ ,  $\eta_d \approx 0.9$  (12),  $\Delta f = 0.125 \text{ Hz}$ ,  $R_1 = 6.67 \times 10^6 \Omega$

<sup>2</sup> $i_d = 1.2 \times 10^{-12} \text{A}$ ,  $B = 1.42$ ,  $G = 2.0 \times 10^5$ ,  $\eta_d \approx 0.9$  (12),  $\Delta f = 0.125 \text{ Hz}$ ,  $R_1 = 6.67 \times 10^6 \Omega$

<sup>3</sup> $i_d = 1.0 \times 10^{-15} \text{A}$  (13), other parameters as in note 2

<sup>4</sup> $i_d = 2.5 \times 10^{-9} \text{A}$ ,  $\Delta f = 0.125 \text{ Hz}$ ,  $R_1 = 6.67 \times 10^6 \Omega$ ,  $T_r = 296 \text{ K}$

<sup>5</sup> $R_d = 7.1 \times 10^5 \Omega$ ,  $T_d = 296 \text{ K}$ ,  $R_1 = 6.67 \times 10^6 \Omega$ ,  $T_r = 296 \text{ K}$ ,  $\Delta f = 0.125 \text{ Hz}$

<sup>6</sup> $R_d = 3.2 \times 10^6 \Omega$ ,  $T_d = 243 \text{ K}$ ,  $R_1 = 6.67 \times 10^6 \Omega$ ,  $T_r = 296 \text{ K}$ ,  $\Delta f = 0.125 \text{ Hz}$

<sup>7</sup> $R_d = 6.67 \times 10^6 \Omega$ ,  $i_a = 1 \times 10^{-14} \text{ A Hz}^{-1/2}$  (14),  $V_a = 1.5 \times 10^{-8} \text{ V Hz}^{-1/2}$  (14),  $\Delta f = 0.125 \text{ Hz}$

<sup>8</sup> typical noise of  $1.0 \times 10^{-8} \text{ V Hz}^{-1/2}$  (15),  $\Delta f = 0.125 \text{ Hz}$

Table III. Calculated Contribution to White Noise Output:  
Photodiode Array (-17°C)

<u>Noise Source</u>	<u>Calculated Noise Values (rms)</u>	
	<u># of Electrons</u>	<u>Fraction of Saturation</u>
Shot (dark) <sup>1</sup>	$1.4 \times 10^3$	$1.6 \times 10^{-5}$
Pixel Readout <sup>2</sup>	$9.4 \times 10^2$	$1.1 \times 10^{-5}$
Preamplifier <sup>3</sup>	$1.3 \times 10^3$	$1.5 \times 10^{-5}$
Scaling Preamplifier <sup>4</sup>	$7.3 \times 10^2$	$8.3 \times 10^{-6}$
Quantization	$6.2 \times 10^3$	$7.0 \times 10^{-5}$

$$^1 i_d = 8 \times 10^{-14} \text{ A } (-17^\circ\text{C}) \text{ (16), } t = 4.0 \text{ s}$$

$$^2 C_p = 2 \text{ pF, } C_{vc} = 1.2 \text{ pF (16), } T_d = 256 \text{ K}$$

$$^3 i_a \approx 1.5 \times 10^{-15} \text{ A [estimated from the gate current specification (17)],}$$

$$t_p = 5.6 \times 10^{-5} \text{ s (pixel clock rate = 18 kHz), } v_a = 2.7 \times 10^{-6} \text{ V (17),}$$

$$C \approx 75 \text{ pF (video line capacitance = 24 pF (16), amplifier capacitance = 8 pF (17), cable capacitance } \approx 1 \text{ pF/cm for } \sim 40 \text{ cm)}$$

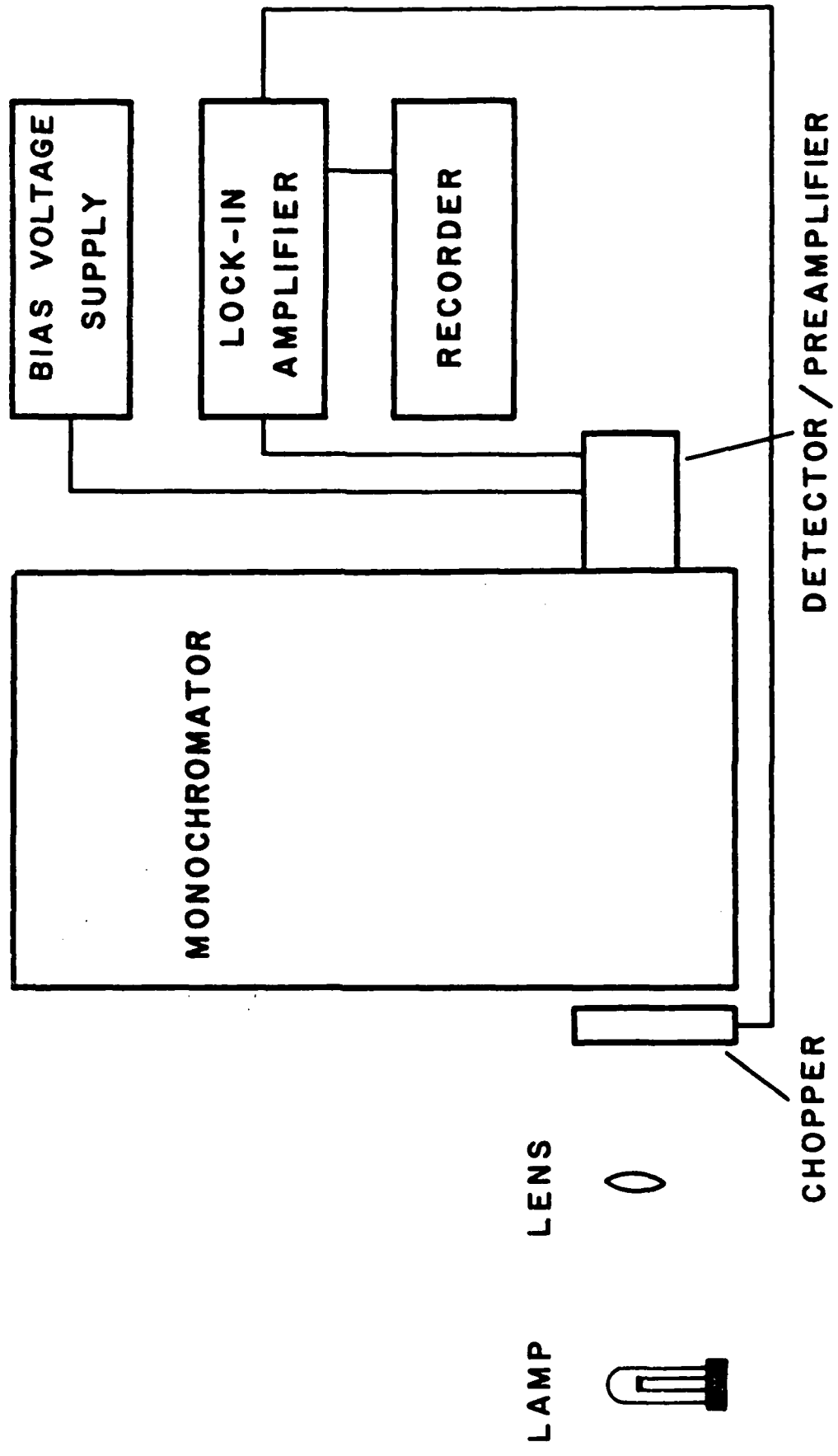
$$^4 v_a = 2.5 \times 10^{-8} \text{ VHz}^{-1/2} \text{ (18), } \Delta f = 1 \times 10^6 \text{ Hz, saturation voltage = 3 V,}$$

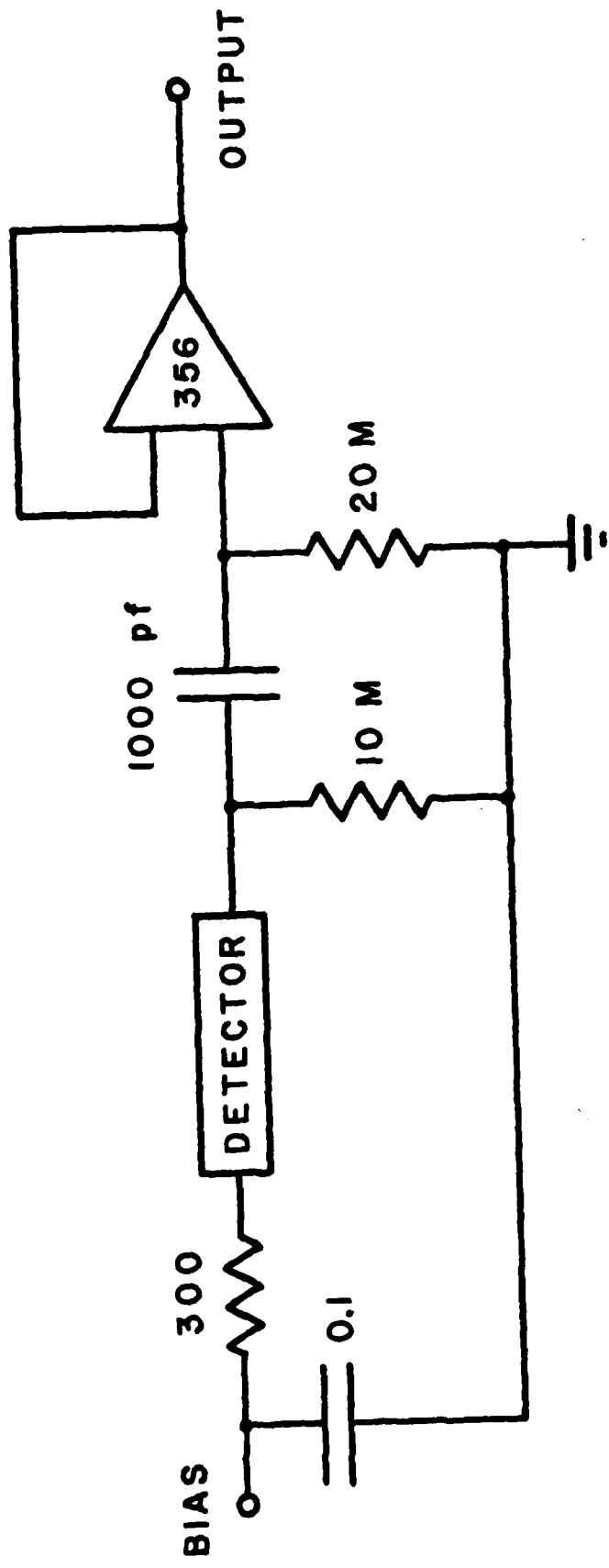
$$i_{a1} R_1 \text{ is negligible}$$

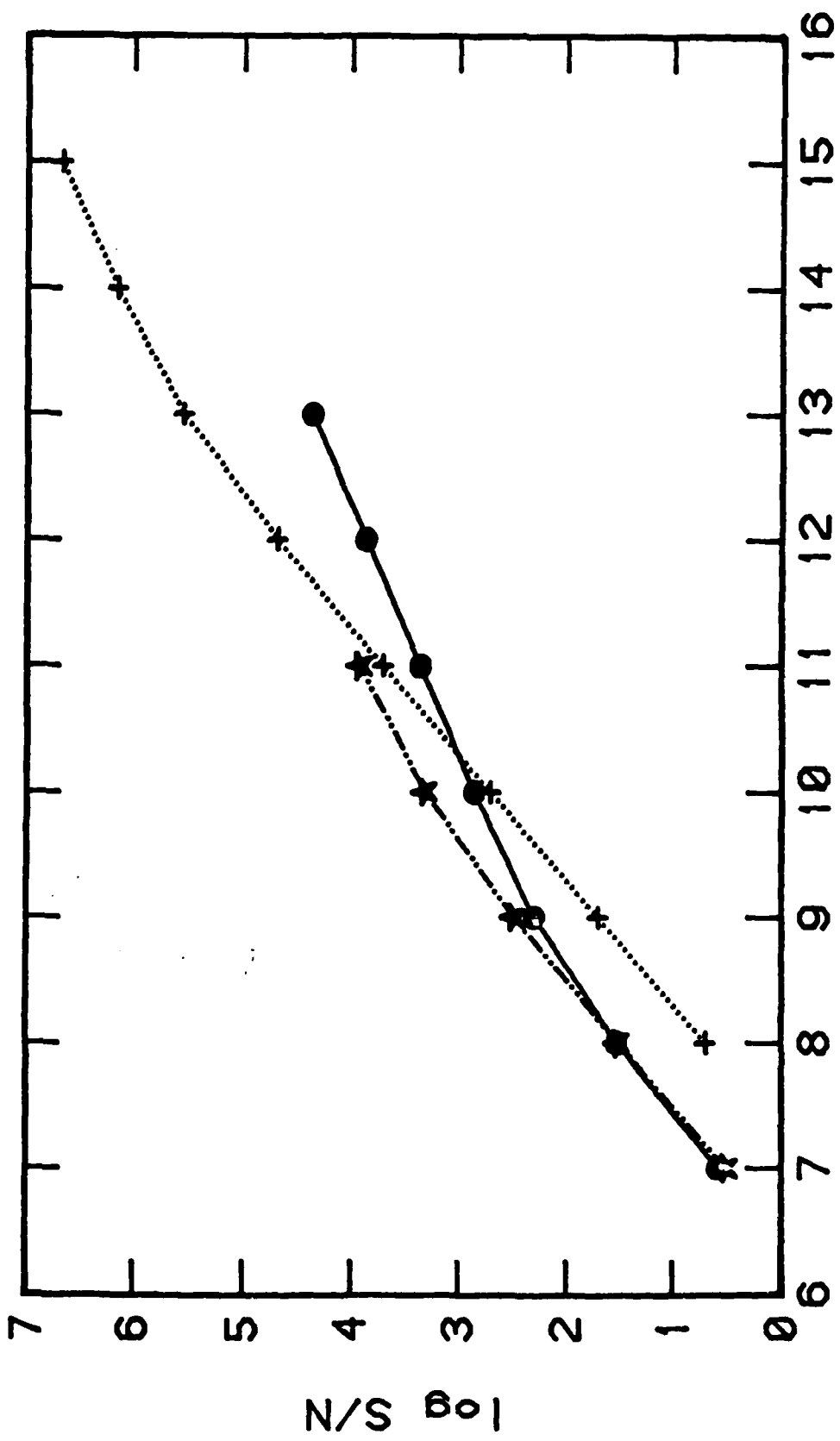
Table IV. Signal and Noise Measurements

	<u>R636 PMT (23°C)</u>	<u>7102 PMT (23°C)</u>	<u>7102 PMT (cooled)</u>	<u>PD (23°C)</u>	<u>PCD (23°C)</u>	<u>PCD (-30°C)</u>	<u>PDA (-20°C)</u>
Signal (V)	$2.6 \times 10^{-3}$	$3.1 \times 10^{-3}$	$3.8 \times 10^{-3}$	$6.7 \times 10^{-5}$	—	$6. \times 10^{-6}$	$2.3 \times 10^{-1}$
Noise (V rms)	$1.1 \times 10^{-5}$	$1.2 \times 10^{-4}$	$4.6 \times 10^{-6}$	$1.2 \times 10^{-7}$	$1.8 \times 10^{-7}$	$3.5 \times 10^{-7}$	$9.3 \times 10^{-1}$
S/N	$2.4 \times 10^2$	$2.6 \times 10^1$	$8.2 \times 10^2$	$5.6 \times 10^2$	—	$1.7 \times 10^1$	$2.5 \times 10^2$
S/N at DC	$3.1 \times 10^2$	$5.0 \times 10^1$	$1.7 \times 10^3$				

\* Signal and noise for the PDA are given in terms of fraction of saturation.

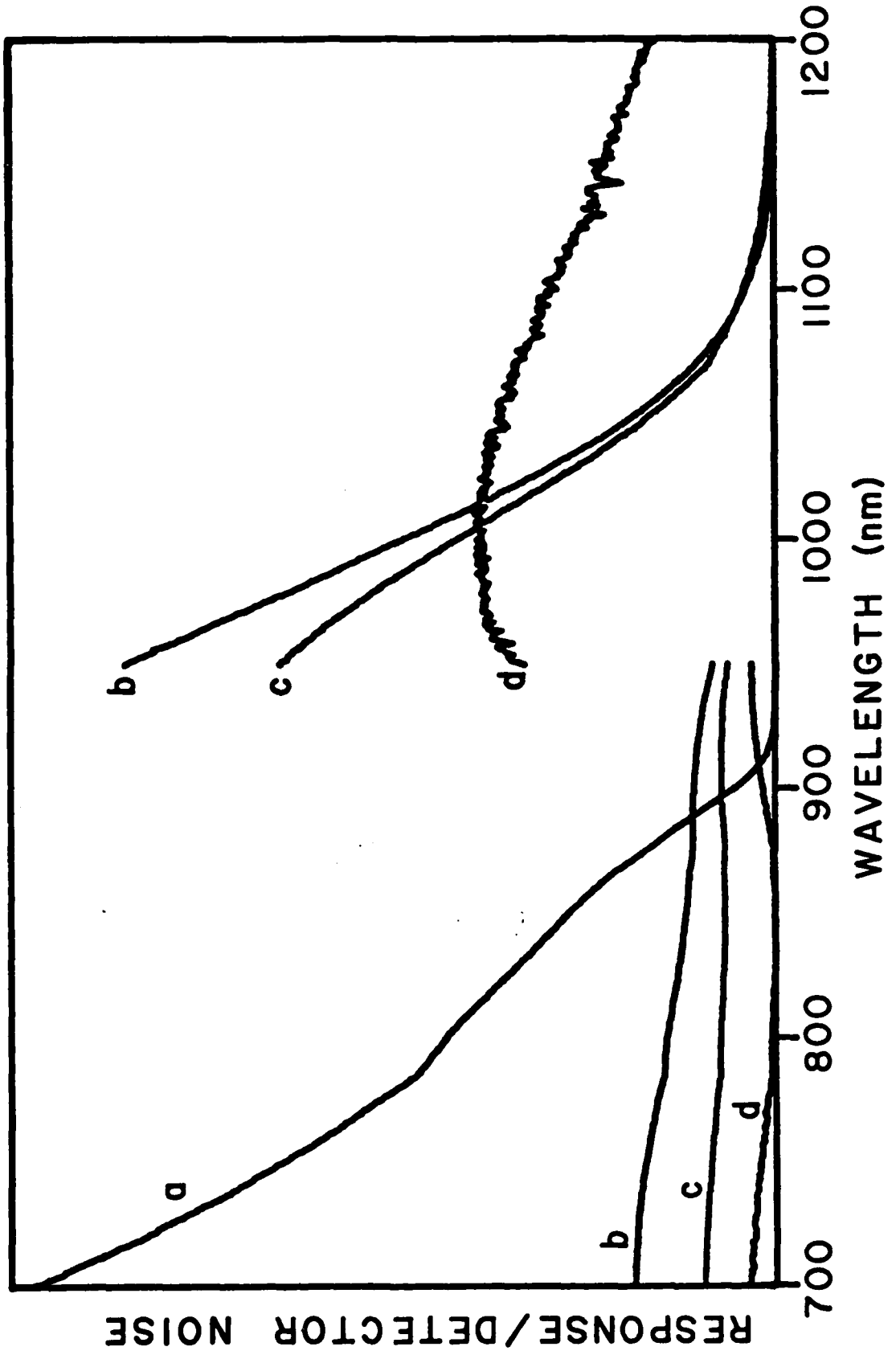






log PHOTON FLUX (photons s<sup>-1</sup> cm<sup>-2</sup>)

log S/N



TECHNICAL REPORT DISTRIBUTION LIST, GEN

	<u>No. Copies</u>		<u>No. Copies</u>
Office of Naval Research Attn: Code 413 800 N. Quincy Street Arlington, Virginia 22217	2	Naval Ocean Systems Center Attn: Technical Library San Diego, California 92152	1
ONR Pasadena Detachment Attn: Dr. R. J. Marcus 1030 East Green Street Pasadena, California 91106	1	Naval Weapons Center Attn: Dr. A. B. Amster Chemistry Division China Lake, California 93555	1
Commander, Naval Air Systems Command Attn: Code 310C (H. Rosenwasser) Washington, D.C. 20360	1	Scientific Advisor Commandant of the Marine Corps Code RD-1 Washington, D.C. 20380	1
Naval Civil Engineering Laboratory Attn: Dr. R. W. Drisko Port Hueneme, California 93401	1	Dean William Tolles Naval Postgraduate School Monterey, California 93940	1
Superintendent Chemistry Division, Code 6100 Naval Research Laboratory Washington, D.C. 20375	1	U.S. Army Research Office Attn: CRD-AA-IP P.O. Box 12211 Research Triangle Park, NC 27709	1
Defense Technical Information Center Building 5, Cameron Station Alexandria, Virginia 22314	12	Mr. Vincent Schaper DTNSRDC Code 2830 Annapolis, Maryland 21402	1
DTNSRDC Attn: Dr. G. Bosmajian Applied Chemistry Division Annapolis, Maryland 21401	1	Mr. John Boyle Materials Branch Naval Ship Engineering Center Philadelphia, Pennsylvania 19112	1
Naval Ocean Systems Center Attn: Dr. S. Yamamoto Marine Sciences Division San Diego, California 91232	1	Mr. A. M. Anzalone Administrative Librarian PLASTEC/ARRADCOM Bldg 3401 Dover, New Jersey 07801	1

TECHNICAL REPORT DISTRIBUTION LIST, 051B

Dr. M. B. Denton  
Department of Chemistry  
University of Arizona  
Tucson, Arizona 85721

Dr. R. A. Osteryoung  
Department of Chemistry  
State University of New York  
Buffalo, New York 14214

Dr. J. Osteryoung  
Department of Chemistry  
State University of New York  
Buffalo, New York 14214

Dr. B. R. Kowalski  
Department of Chemistry  
University of Washington  
Seattle, Washington 98105

Dr. H. Freiser  
Department of Chemistry  
University of Arizona  
Tucson, Arizona 85721

Dr. H. Chernoff  
Department of Mathematics  
Massachusetts Institute of Technology  
Cambridge, Massachusetts 02139

Dr. A. Zirino  
Naval Undersea Center  
San Diego, California 92132

Professor George H. Morrison  
Department of Chemistry  
Cornell University  
Ithaca, New York 14853

Dr. Alan Bewick  
Department of Chemistry  
Southampton University  
Southampton, Hampshire  
ENGLAND 5095NA

Dr. S. P. Perone  
Lawrence Livermore Laboratory L-370  
P.O. Box 808  
Livermore, California 94550

Dr. L. Jarvis  
Code 6100  
Naval Research Laboratory  
Washington, D.C. 20375

Dr. G. M. Hieftje  
~~Department of Chemistry~~  
~~Indiana University~~  
Bloomington, Indiana 47401

Dr. Christie G. Enke  
Department of Chemistry  
Michigan State University  
East Lansing, Michigan 48824

Dr. D. L. Venezky  
Naval Research Laboratory  
Code 6130  
Washington, D.C. 20375

Walter G. Cox, Code 3632  
Naval Underwater Systems Center  
Building 148  
Newport, Rhode Island 02840

Professor Isiah M. Warner  
Department of Chemistry  
Emory University  
Atlanta, Georgia 30322

Dr. Kent Eisentraut  
Air Force Materials Laboratory  
Wright-Patterson AFB, Ohio 45433

Dr. Adolph B. Amster  
Chemistry Division  
Naval Weapons Center  
China Lake, California 93555

Dr. B. E. Douda  
Chemical Sciences Branch  
Code 50 C  
Naval Weapons Support Center  
Crane, Indiana 47322

Dr. John Eyler  
Department of Chemistry  
University of Florida  
Gainesville, Florida 32611

TECHNICAL REPORT DISTRIBUTION LIST, 051B

Professor J. Janata  
Department of Bioengineering  
University of Utah  
Salt Lake City, Utah 84112

Dr. J. DeCorpo  
NAVSEA  
Code 05R14  
Washington, D.C. 20362

Dr. Charles Anderson  
Analytical Chemistry Division  
Athens Environmental Laboratory  
College Station Road  
Athens, Georgia 30613

Dr. Ron Flemming  
B 108 Reactor  
National Bureau of Standards  
Washington, D.C. 20234

Dr. David M. Hercules  
Department of Chemistry  
University of Pittsburgh  
Pittsburgh, Pennsylvania

Dr. Frank Herr  
Office of Naval Research  
Code 422CB  
800 N. Quincy Street  
Arlington, Virginia 22217

Professor E. Keating  
Department of Mechanical Engineering  
U.S. Naval Academy  
Annapolis, Maryland 21401

Dr. M. H. Miller  
1133 Hampton Road  
Route 4  
U.S. Naval Academy  
Annapolis, Maryland 21401

Dr. Clifford Spiegelman  
National Bureau of Standards  
Room A337 Bldg. 101  
Washington, D.C. 20234

Dr. Denton Elliott  
AFOSR/NC  
Bolling AFB  
Washington, D.C. 20362

Dr. B. E. Spielvogel  
Inorganic and Analytical Branch  
P.O. Box 12211  
Research Triangle Park, NC 27709

Ms. Ann De Witt  
Material Science Department  
160 Fieldcrest Avenue  
Raritan Center  
Edison, New Jersey 08818

Dr. A. Harvey  
Code 6110  
Naval Research Laboratory  
Washington, D.C. 20375

Dr. John Hoffsommer  
Naval Surface Weapons Center  
Building 30 Room 208  
Silver Spring, Maryland 20910

Mr. S. M. Hurley  
Naval Facilities Engineering Command  
Code 032P  
200 Stovall Street  
Alexandria, Virginia 22331

Ms. W. Parkhurst  
Naval Surface Weapons Center  
Code R33  
Silver Spring, Maryland 20910

Dr. M. Robertson  
Electrochemical Power Sources Division  
Code 305  
Naval Weapons Support Center  
Crane, Indiana 47522

CDR Andrew T. Zander  
10 Country Club Lane  
ONR Boston  
Plaistow, New Hampshire 03865

DL/413/83/01  
051B/413-2

TECHNICAL REPORT DISTRIBUTION LIST, 051B

Dr. Robert W. Shaw  
U.S. Army Research Office  
Box 12211  
Research Triangle Park, NC 27709

Dean William Tolles  
Naval Post Graduate School  
Spanaue1 Hall  
Monterey, California 93940

Dr. Marvin Wilkerson  
Naval Weapons Support Center  
Code 30511  
Crane, Indiana 47522

Dr. H. Wohltjen  
Naval Research Laboratory  
Code 6170  
Washington, D.C. 20375

Dr. J. Wyatt  
Naval Research Laboratory  
Code 6110  
Washington, D.C. 20375

END

FILMED

3-84

DTIC